Accepted Manuscript published as ERC-18-0538.R1. Accepted for publication: 15-Jan-2019

SHH pathway inhibition is protumourigenic in adamantinomatous craniopharyngioma

G. Carreno[1], J.K.R. Boult[2], J. Apps[1], J.M. Gonzalez-Meljem[1, 3], S. Haston[1], R. Guiho[1], C. Stache, L.S. Danielson[4], A. Koers[4], L.M. Smith[4], A. Virasami[5], L. Panousopoulos[1], M. Buchfelder[6], T. Jacques[1,5], L. Chesler[4], S.P. Robinson[2], and J.P. Martinez-Barbera[1,*]

1. Developmental Biology and Cancer Programme, Birth Defects Research Centre, Great Ormond Street Institute of Child Health, University College London, London, UK
2. Division of Radiotherapy and Imaging, The Institute of Cancer Research, London, UK
3. Basic Research Department, Instituto Nacional de Geriatría, Anillo Periférico 2767, Magdalena Contreras,10200, Mexico City, Mexico
4. Paediatric Solid Tumour Biology and Therapeutics Team, Division of Clinical Studies and Cancer Therapeutics Division, The Institute of Cancer Research, London, UK
5. Department of Histopathology, Great Ormond Street Hospital for Children, NHS Foundation Trust, London, UK
6. Department of Neurosurgery, University Hospital Erlangen, Erlangen, Germany.

* Corresponding author: j.martinez-barbera@ucl.ac.uk

Running title: SHH Pathway inhibition in craniopharyngioma

Key words: craniopharyngioma, pituitary, SHH, vismodegib, tumour

Word Count: 4441

ABSTRACT

Pharmacological inhibition of the sonic hedgehog (SHH) pathway can be beneficial against certain cancers but detrimental in others. Adamantinomatous craniopharyngioma (ACP) is a relevant pituitary tumour, affecting children and adults, that is associated with high morbidity and increased mortality in long-term follow up. We have previously demonstrated overactivation of the SHH pathway in both human and mouse ACP. Here, we show that this activation is ligand dependent and induced by the expression of SHH protein in a small proportion of tumour cells. We investigate the functional relevance of SHH signalling in ACP through magnetic resonance imaging (MRI) -guided preclinical studies using an ACP mouse model. Treatment with vismodegib, a clinically approved SHH pathway inhibitor, results in a significant reduction in median survival due to premature development of highly proliferative and vascularised undifferentiated tumours. Reinforcing the mouse data, SHH pathway inhibition in human ACP leads to a significant increase in tumour cell proliferation both ex vivo, in explant cultures, and in vivo, in a patient-derived xenograft model. Together, our results demonstrate a protumourigenic effect of vismodegib-mediated SHH pathway inhibition in ACP.

Accepted Manuscript published as ERC-18-0538.R1. Accepted for publication: 15-Jan-2019

INTRODUCTION

Adamantinomatous craniopharyngiomas (ACPs) are benign tumours of the sellar region that are associated with high morbidity and increased mortality in long-term follow up. They constitute the most common non-neuroepithelial brain tumour in children (peak diagnosis at 5–14 years) and can also develop in adults (peak diagnosis 50–74 years). ACPs display clinically aggressive behaviour by invading vital surrounding structures such as the hypothalamus and optic chiasm, which complicates surgical resection leading to severe postoperative sequelae. Currently there are no targeted molecular treatments for these patients (Karavitaki and Wass, 2008, Muller et al., 2017) The majority of human ACPs carry somatic mutations in *CTNNB1*, which result in the expression of a degradation-resistant form of β-catenin and activation of the WNT/β-catenin pathway (Sekine et al., 2002, Kato et al., 2004, Buslei et al., 2005, Brastianos et al., 2014, Apps et al., 2018).

The expression of functionally equivalent mutant β-catenin in either pituitary embryonic precursors (*Hesx1*$^{Cre/+}$;*Ctnnb1*$^{lox(ex3)/+}$ mice) or adult pituitary stem cells (*Sox2*$^{CerERT2/+}$;*Ctnnb1*$^{lox(ex3)/+}$ mice) results in the formation of tumours resembling human ACP (Andoniadou et al., 2013, Gaston-Massuet et al., 2011). In both models, tumoural pituitaries show the presence of β-catenin-accumulating cells forming clusters, which share a common molecular signature with those found in humans (Gonzalez-Meljem et al., 2017). Our initial studies revealed the upregulation of the sonic hedgehog (SHH) pathway in both mouse and human ACP, a finding confirmed subsequently by independent research (Andoniadou et al., 2012, Gomes et al., 2015, Holsken et al., 2016, Gump et al., 2015). However, the biological function of the SHH pathway in ACP pathogenesis remains unknown to date.

The SHH pathway has been implicated in the pathogenesis of multiple cancers including medulloblastoma, basal cell carcinoma, breast, colon and pancreatic ductal adenocarcinoma (PDAC) (Rimkus et al., 2016). While SHH pathway inhibition has proven beneficial against basal cell carcinoma (Sekulic et al., 2017, Sekulic et al., 2012), it has proven detrimental in other cancers, such as PDAC, where enhanced tumour progression and aggressiveness was observed in both preclinical and clinical trials (Madden, 2012, Catenacci et al., 2015). These discrepancies between favourable or

unfavourable outcomes after SHH pathway inhibition prompted us to assess the functional relevance of the SHH pathway in human ACP. Our preclinical research demonstrates that inhibition of the SHH pathway using vismodegib is not beneficial and is therefore contraindicated in human patients.

MATERIALS AND METHODS

Mice

All experimental protocols were monitored and approved by The Institute of Cancer Research Animal Welfare and Ethical Review Body, in compliance with guidelines specified by the UK Home Office Animals (Scientific Procedures) Act 1986, the United Kingdom National Cancer Research Institute Guidelines for the Welfare of Animals in Cancer Research (Workman et al., 2010) and the ARRIVE guidelines (Karp et al., 2015). Animals were monitored daily and were killed at defined humane end points (i.e. prior to the mice showing signs of severe health deterioration or 20% weight loss). Patient-derived xenografts were generated as previously described (Stache et al., 2015). All mice were housed in compliance with the Home Office Code of Practice. Mice were kept on a 12-hour light/dark cycle and fed *ad libitum* with a complete pelleted mouse diet and with constant access to water.

Hesx1$^{Cre/+}$ mice have been previously described (Andoniadou et al., 2007). The line was maintained on a C57BL/6J background for over 50 generations. Heterozygotes were used for crosses with *Ctnnb1*$^{lox(ex3)/+}$ mice (Harada et al., 1999) to obtain *Hesx1*$^{Cre/+}$and *Ctnnb1*$^{lox(ex3)/+}$ mice (Gaston-Massuet et al., 2011). For xenografts, we used NIH nu/nu were bred in our local Biological Services Unit.

Drug administration

Four week-old male *Hesx1*$^{Cre/+}$*;Ctnnb1*$^{lox(ex3)/+}$ mice were administered vismodegib (Roche) or vehicle in 2% DMSO, 30% PEG 300, 5% Tween 80, ddH_2O via oral gavage at a dose of 100 mg/kg of body weight twice a day (approximately 7.30 am and 4.00 pm).

Human samples

 Accepted Manuscript published as ERC-18-0538.R1. Accepted for publication: 15-Jan-2019

Experiments using human samples were covered by the ethical approval 14 LO 2265 or the ethical approval of specific tissue banks. Human ACP samples were kindly provided by the GOSH Histopathology Department.

***Ex vivo* culture of ACP human tumours**

Explant cultures were performed as previously described (Apps et al., 2018). Small pieces from three different human ACP tumours (approximately 1 mm^3; four replicates per tumour) were placed on 0.2 μM Whatman filters (SLS) in 24 well plates containing 500 μl of media (DMEM-F12 (Gibco), 1% Pen/Strep (Sigma) and 1% FBS (PAA)) supplemented with either Vismodegib 100 μM (Selleckchem) or vehicle (DMSO) and medium was changed every 24h. After 72h, tumour pieces were passed through a Qiashredder column (Qiagen) and processed for total RNA extraction using the RNeasy Micro kit (Qiagen). Approximately 1 μg of total RNA was reverse-transcribed to cDNA using the Transcriptor First Strand cDNA Synthesis Kit and random hexamers (Roche).

Magnetic Resonance Imaging (MRI)

Multi-slice T_2-weighted images were acquired using a 7T Bruker microimaging system with a 3 cm birdcage coil over a 2.5 cm field-of-view (RARE; T_R= 4500 ms, $T_E$eff= 36 ms). MRI was performed on the final day of treatment and at least every 2 weeks thereafter, until mice presented with neurological symptoms or lost condition (Boult et al., 2017).

Histology and immunostaining on histological sections

Immunohistochemistry and immunofluorescence were carried out using the same antibodies, concentrations and retrieval conditions as previously described (Gonzalez-Meljem et al., 2017, Andoniadou et al., 2013, Apps et al., 2018). Immunostaining of SHH protein was also conducted as previously described (Carreno et al., 2017). Section immunostaining was performed as previously described (Andoniadou et al., 2012). Briefly, slides were de-waxed in HistoClear, re-hydrated from 100% EtOH to double distilled MilliQ water and underwent antigen retrieval in an antigen retrieval unit (BioCare Medical Decloaking Chamber NXGEN) for 2 minutes at 95°C. Slides were then

washed in 1X PBT, which consists of 1X PBS and 0.1% Triton X-100. Histological slides were then blocked for 1 hour at RT in blocking buffer and 10% heat inactivated sheep serum (HISS), blocking buffer contains 0.1% Triton X-100, 0.15% glycine, 2mg/ml BSA in 1X PBS. SHH was visualised by using the TSA™ Plus Fluorescein System (Perkin Elmer), following the manufacturer's protocol. Primary and secondary antibodies were diluted into blocking buffer and 1% HISS. Sections were counter stained with 4',6-Diamidino-2-Phenylindole (DAPI) for 5 minutes (1:10,000, Sigma) and mounted onto coverslips with VectaMount (Vector Laboratories). For immunohistochemical stainings, slides were first incubated with an Avidin-Biotinylated Peroxidase Complex (Vector). Chromogenic detection was then conducted by addition of 3,3'-diaminobenzidine (DAB, Vector) for 2-5 minutes and then counterstained with Mayer's hematoxylin (Sigma).

Quantitative analysis of immunofluorescent stainings

The proliferative and mitotic indexes were calculated as a percentage of the Ki67 positive or p-histone H3 positive cells out of the total of DAPI-stained nuclei, respectively. Specifically: In Fig. 2C and D, a total of 15,600 and 16,700 respectively DAPI positive nuclei were counted; 15,213 for vehicle and 13,300 for Vismodegib in Fig. 3D; and 10,037 and 2,332 in Fig. 4D and G. Cells were counted using ImageJ, a Gaussian filter was applied and the cell counter plugin was used. Endomucin positive staining in pixels was analysed as a percentage of the total area using ImageJ.

Quantitative reverse transcriptase PCR (qRT-PCR)

Quantitative reverse transcriptase polymerase chain reaction (qRT-PCR) amplification was performed on murine anterior pituitaries and human tumour samples as previously described (Apps et al., 2018, Gonzalez-Meljem et al., 2017). RNA was extracted from tissues using the RNeasy Micro or Mini Kit (Qiagen). RNA was quantified using 1.2µl of extracted RNA on a NanoDrop 1000 Spectrophotometer. Complementary DNA (cDNA) was retro-transcribed from 1µg of extracted RNA using the iScript Reverse Transcription Supermix for RT-qPCR kit (BioRad). Thermocycling conditions were performed according to manufacturer's instructions. qRT-PCR was performed using 64 iTaq Universal SYBR Green Supermix (BioRad), thermocycling conditions were performed

 Accepted Manuscript published as ERC-18-0538.R1. Accepted for publication: 15-Jan-2019

according to manufacturer's instructions. Analysis was performed using CFX Manager BioRad software. 3µl of the amplified product was run by gel electrophoresis in order to visualise correct product size. Relative quantitation of the target gene was performed against glyceraldehyde 3-phospate dehydrogenase (*Gapdh*) as the house-keeping gene in murine and human samples. The average Ct values were calculated for the control and test sample genes. ΔCt was calculated by subtracting the Ct of the house-keeping gene from the target gene Ct values for both test and control samples. ΔΔCt was then calculated as the ratio of expression between the test and control samples. Finally, the fold change was calculated by 2 –ΔΔCt for each sample. *SHH, GLI1* and *PTCH1* levels were measured using the Qiagen QuantiTect Primers (Cat. QT00205625, QT00060501, QT00075824). Murine *Shh* and *Gli*1levels were measured with the Qiagen QuantiTect Primers (Cat. QT00122479, QT00173537).

Murine pituitary adherent clonogenic cell culture

Clonogenic assays were performed on murine tumoural pituitaries as described (Carreno et al., 2017, Haston et al., 2017, Gaston-Massuet et al., 2011). Pituitaries were dissected using aseptic forceps and the posterior pituitary was removed. After mincing with forceps, the remaining tissue was placed into 200 µl of enzyme mix, which consisted of Hanks' Balanced Salt Solution (HBSS, Gibco), 0.5% w/v Collagenase (Worthington), 50µg/ml DNAase I (Worthington), 1% Fungizone and 0.1X trypsin (Sigma), for 4 hours in a 37°C water bath. HBSS was added to make a final volume of 500µl post incubation and the solution was triturated into a single cell suspension. Once single cell suspensions were achieved, 9.5ml of HBSS was added and the cells spun down for 5 minutes at 1000rpm. Cells were re-suspended in growth medium, which consisted of DMEM/F12, 5% FCS, 1% PenStrep, 20ng/ml human recombinant bFGF (R&D Systems) and 50 ng/ml cholera toxin. Cells were plated at clonal density in a 6-well plate at 2000, 4000 and 8000 cells per well. Fresh bFGF was added after 2 days, medium was then changed on the third day and every 3 days after colony establishment. Colony counting was conducted after 7 days in culture. Colonies were washed with PBS and fixed for 20 minutes with 4% PFA, washed again in PBS and stained with Harris haematoxylin for 15 minutes at room temperature.

178

179 **Xenografts**

180 Patient-derived xenograft (PDX) mice were generated as described (Stache et al., 2015).
181 NIH nu/nu mice were anesthetised with 2% isoflurane and the top of the head was disinfected. An
182 ~1cm incision was made to the skin of the head to expose the skull. The incision was treated with
183 10% xylocaine. 30% H_2O_2 was applied to the skull to remove the periosteal membranes. A 1 mm in
184 diameter hole was bored into the skull, 1 mm left and 1 mm posterior of the Bregma. Human ACP
185 tumour tissue was dissected into 1-2 mm^3 pieces and these were inserted into the cortex using forceps.
186 The skin was then sutured to close the wound. The surgical area was disinfected again. Mice were
187 placed on a heated mat and monitored until recovery.

188

189 **Statistics**

Independent unpaired t-tests and one-way ANOVA were used to analyse the data from the qRT-PCR and proliferative assays using GraphPad Prism. Immunofluorescence was analysed using Image J. $P<0.05$ was considered statistically significant. The "n" value indicated throughout the text refers to number of biological replicas, i.e. different mice, pituitaries or tumour samples. Technical replicas, i.e. number of repeats for the same sample, were three for the qRT-PCR experiments. In general, we have not performed power calculations to estimate the sample size. In most of the quantitative experiments, we have used at least three biological replicas (e.g. Fig. 1C, Fig. 3D,E), often 6 or more (e.g. Fig. 1D, Fig. 2C-F). Only in the xeno-transplantation experiments, have we used two human tumours (Fig. 4E). Many of these experiments use embryos or mouse and human tumours, which are samples not readily available. For the preclinical trial (Fig. 1F), we performed a power calculation, based on pilot experiments. A total of 12 mice per group was decided to compensate for sample attrition.

190

191 **RESULTS**

192 **SHH protein is expressed in mouse and human ACP leading to the paracrine activation of the**
193 **SHH pathway**

Accepted Manuscript published as ERC-18-0538.R1. Accepted for publication: 15-Jan-2019

The expression of SHH at the mRNA level in the β-catenin-accumulating cell clusters and activation of the SHH pathway in human ACP have been thoroughly documented (Andoniadou et al., 2012, Gomes et al., 2015, Gump et al., 2015, Holsken et al., 2016). However, the SHH protein has not been identified in human or mouse ACP. Double immunostaining revealed the co-localisation of β-catenin and SHH protein in clusters of both human and mouse ACP **(Figs. 1A and 1B, respectively)**. qRT-PCR revealed that *Shh* mRNA expression was increased in *Hesx1*$^{Cre/+}$*;Ctnnb1*$^{lox(ex3)/+}$ mutant mice relative to age-matched *Ctnnb1*$^{lox(ex3)/+}$ controls at one (134±1 -fold), four (125±1 -fold) and eight (68 -fold) weeks of age (n=3-5 samples/group, $p<0.0001$, Student's t-test). The expression of the SHH pathway target gene *Gli1* was also up-regulated at all stages in mutant pituitaries compared to controls (one week: 15.3±0.2 -fold $p=0.018$; four weeks: 8.7±0.1 -fold; eight weeks: 4.9±0.3-fold; n=3-5 samples/group; $p<0.0001$; Student's t-test) **(Fig. 1C)**. Note that a similar decreasing trend in *Gli1* and *Shh* mRNA expression was observed over time (**Fig. 1C**). Since mutations in the components of the SHH pathway have not been identified in humans (Brastianos et al., 2014, Apps et al., 2018) or mouse ACP (Gonzalez-Meljem et al., 2017), our data suggest that the SHH pathway is activated in ACP in a ligand-dependent manner.

Inhibition of the SHH pathway in a genetically modified murine model of ACP results in reduced survival and increased tumourigenesis

To assess the role of the SHH pathway in the pathogenesis of ACP, we performed a magnetic resonance imaging (MRI)-guided preclinical trial using the smoothened (SMO) inhibitor vismodegib in the *Hesx1*$^{Cre/+}$*;Ctnnb1*$^{lox(ex3)/+}$ ACP mouse model. Clinical trials have demonstrated that treatment with vismodegib results in long-term responses in patients with advanced basal cell carcinoma (Sekulic et al., 2017, Sekulic et al., 2012) and this inhibitor is currently being used in numerous ongoing clinical trials for other human cancers (Rimkus et al., 2016).

Pharmacokinetic studies in mice have shown that serum levels of vismodegib decrease after 12 hours and suggested that a twice a day dosing regime leads to more permanent pathway inhibition (Wong et al., 2011). An administration dose of 100 mg/kg of body weight was chosen as it is the

highest non-toxic dose identified in the literature (Wong et al., 2011). A dosing regimen of twice a day for seven days was chosen as it was hypothesised that any pharmacological effect on the SHH pathway would be evident after seven days. This dosing regimen revealed an overall reduction in relative *Gli1* mRNA levels in the vismodegib-treated tumoural pituitaries compared to vehicle-treated control pituitaries, which did not reach significance (vehicle: 2.5-fold, vismodegib: 1.5-fold, n=8; p=0.35, ANOVA) (**Fig. 1D**). We noted a high degree of variability in *Gli1* expression levels in the vehicle-control group as well as untreated *Hesx1*$^{Cre/+}$*;Ctnnb1*$^{lox(ex3)/+}$ mice (2.1-fold relative to *Ctnnb1*$^{lox(ex3)/+}$ controls, n=7 mice), with some animals showing much higher *Gli1* levels than others, suggesting a similarly inherent heterogeneity in the ACP mouse model to that reported in human ACP (Gomes et al., 2015). *Gli1* expression mRNA levels were lower and more uniform with vismodegib treatment. We did not evaluate GLI1 expression at the protein level.

For the preclinical trial, *Hesx1*$^{Cre/+}$*;Ctnnb1*$^{lox(ex3)/+}$ mice were dosed twice a day with 100 mg/kg of body weight of vismodegib or vehicle (11 and 12 mice, respectively) for a total of 56 doses over 28 days (the maximum allowed by UK animal welfare authorities) **(Fig. 1E)**. Treated mice were monitored by MRI and killed at a defined humane endpoint (i.e. prior to the mice showing signs of severe health deterioration or 20% weight loss). Surprisingly, a significant decrease in survival was observed in the vismodegib-treated animals in comparison with vehicle-treated controls (11.9 weeks vs. 33.3 weeks; p=0.049, log rank test) **(Fig. 1F)**.

T_2-weighted MRI throughout the trial up until each humane end point for both treated and vehicle groups demonstrated no significant differences in tumour phenotype and size of total and solid tumour volume **(Fig. 2A)**. In other words, the vismodegib-treated mice did not develop larger tumours; at the humane end point tumours were similar in size. MRI revealed tumour enlargement and heterogeneity in both groups prior to the development of hyperintense cysts, expansion of a solid portion of the tumour and presentation of hypointense haemorrhagic regions, consistent with our previous imaging studies (Boult et al., 2017). Furthermore histologically, tumours showed no gross morphological differences between the groups **(Fig. 2B)**. However, the MRI data revealed that the doubling time of the solid component of the tumours was shorter in vismodegib-treated tumours compared with controls (vismodegib: 8.1±1days; n=6; vehicle: 15.3±3days; n=7; p=0.044; Student's

 Accepted Manuscript published as ERC-18-0538.R1. Accepted for publication: 15-Jan-2019

t-test) **(Fig. 2F).** In agreement with these observations, the Ki67 proliferative index was increased in the vismodegib treated group (41.3±7%, n=10) compared with controls (27.4±5.5%, n=9) (p=0.0002, Student's t test) **(Fig. 2C)**. The mitotic index, measured by phospho-Histone H3 (pHH3) immunofluorescence, was also increased in the vismodegib treated group (vismodegib: 6.5±3%; n=10; vehicle: 3.6±0.8%; n=9; p=0.016; Student's t-test) **(Fig. 2D)**. Vismodegib treatment led to increased vasculogenesis, as assessed by immunofluorescence staining against the endothelial marker endomucin (fluorescent area: 7.8±2% in vismodegib-treated group; 5.4±1.4% in control group; n=6; p=0.0319; Student's t-test) **(Fig. 2E)**. Together, these results suggest that chemical SHH pathway inhibition using vismodegib in *Hesx1$^{Cre/+}$;Ctnnb1$^{lox(ex3)/+}$* mice results in formation of aggressive tumours.

Vismodegib-treated *Hesx1$^{Cre/+}$;Ctnnb1$^{lox(ex3)/+}$* mouse pituitaries develop tumours prematurely and show increased numbers of clonogenic cells

We hypothesised that inhibiting the SHH pathway could lead to an increase in the number of cells with clonogenic tumour cells within, potentially tumour-initiating cells. Four week-old *Hesx1$^{Cre/+}$;Ctnnb1$^{lox(ex3)/+}$* mice were treated with either vismodegib (100 mg/kg of body weight) or vehicle for 7 days, after which tumoural pituitaries were dissected and subjected to either histological analysis or assessment of the clonogenic potential as previously described (Gaston-Massuet et al., 2011, Andoniadou et al., 2013) **(Fig. 3A)**. H&E staining identified tumour lesions in vismodegib-treated *Hesx1$^{Cre/+}$;Ctnnb1$^{lox(ex3)/+}$* pituitaries (3/3 pituitaries, **Fig. 3B, arrows**), which were not present in the vehicle treated mice (0/3 pituitaries). These tumoural lesions were synaptophysin negative, suggesting loss of differentiation into hormone-producing cells **(Fig. 3C)**, consistent with previous observations in mouse and human ACP. Furthermore, vismodegib-treated tumoural pituitaries showed a higher Ki67 proliferative index compared with controls (controls: 3±1.2%; vismodegib: 8.8±1.0%; n=3; p=0.0037; Student's t-test) **(Fig. 3D)**. We have previously shown the expansion of clonogenic SOX2 positive tumour cells in the *Hesx1$^{Cre/+}$;Ctnnb1$^{lox(ex3)/+}$* mice (Andoniadou et al., 2013, Gaston-Massuet et al., 2011). Immunofluorescent staining revealed an elevation in SOX2 expression in the vismodegib treated *Hesx1$^{Cre/+}$;Ctnnb1$^{lox(ex3)/+}$* pituitaries compared with vehicle-treated controls.

Moreover, dissociation of tumoural pituitaries into single cell suspensions and culture in stem cell-promoting media showed a significant increase in the numbers of colonies in vismodegib-treated animals relative to controls (vehicle: 2597±98; vismodegib: 4924±167; n=3; p=0.0003; Student's t-test) **(Figs. 3E,F)**. Currently, there is no ACP primary cell culture that maintains the mutation sustaining cells throughout passages. Together, these results suggest that the inhibition of the SHH pathway leads to an increase in clonogenic tumour cells, with increased proliferative capacity, which promotes the development of premature tumour lesions **(Fig. 3G)**.

Inhibition of the SHH pathway in human ACP tumours leads to increased proliferation

Finally, we assessed the relevance of the murine studies in human ACP. Small pieces of human ACP tumours (1-2mm^3) were cultured *ex vivo* in the presence of vismodegib or vehicle and after 3 days, tissue was analysed **(Fig. 4A)** (Apps et al., 2018). Vismodegib treatment resulted in the overall down-regulation of the SHH pathway, as assessed by qRT-PCR against *GLI1*, *PTCH1* and *SHH* **(Fig. 4B)**, and the concomitant increase of the proliferative index (38.7±12%) relative to the vehicle controls (5.1±3%; n= 3; p=0.0085; Student's t-test) **(Figs. 4C,D)**. To assess the effects of vismodegib *in vivo,* small fragments of human ACP were engrafted into the brains of 20 immunodeficient mice **(Fig. 4E)**. After 3 months, mice were divided into two groups (10 mice/group) and administered 100 mg/kg of body weight of vismodegib or vehicle, twice a day for 3 weeks, after which brains were collected for histological analysis. Immunofluorescent staining revealed a significant increase in the Ki67 proliferative index in Vismodegib-treated xenograft mice (12.7±2%, n=4) relative to the vehicle-treated controls (1.8±0.5%, n=3) ($p<0.0001$, Student's t-test) **(Figs. 3F,G)**.

DISCUSSION

The main highlight of this research is the demonstration that the inhibition of the SHH pathway using vismodegib, a well-established SMO inhibitor used in the clinic (De Smaele et al., 2010), results in premature tumour formation and increased tumour cell proliferation in both

 Accepted Manuscript published as ERC-18-0538.R1. Accepted for publication: 15-Jan-2019

304 genetically engineered and patient-derived xenograft mouse models. These data suggest that the use
305 of vismodegib and potentially other SMO inhibitors is contraindicated in ACP patients.

306 The activation of the SHH pathway in human ACP was initially documented from research in
307 the *Hesx1*$^{Cre/+}$;*Ctnnb1*$^{loxex3/+}$ mouse model of ACP. The presence of mRNA expression was
308 demonstrated in five human ACP tumours (Andoniadou et al., 2012). These results were extended
309 further in a larger cohort of tumours by Gomes et al., who revealed the expression of GLI1, GLI3,
310 SUFU and SMO in human ACP at the protein level (Gomes et al., 2015). More recently the activation
311 of the SHH pathway has been demonstrated in gene expression analyses of ACP (Holsken et al.,
312 2016, Donson et al., 2017, Apps et al., 2018). Mutations in components of the SHH pathway (i.e. loss-
313 of-function mutations in PTCH1 or gain-of-function mutations in SMO) have not been identified in
314 independent sequencing efforts neither in human nor in mouse ACP, suggesting that the SHH
315 pathway may be activated in a paracrine manner (Theunissen and de Sauvage, 2009). Here, we
316 extend these observations by demonstrating the presence of SHH protein within the beta-catenin-
317 accumulating cell clusters, hence reinforcing the idea that the SHH pathway is activated in a ligand-
318 dependent fashion. Of relevance, we have recently shown that these clusters contain senescent cells
319 and act as signalling hubs within the tumours by activating the expression of numerous secreted
320 factors, including SHH, FGF, EGF, BMP, TGF beta among others (Apps et al., 2018, Gonzalez-
321 Meljem et al., 2017).

322 We show that treatment with vismodegib leads to accelerated tumourigenesis with tumours
323 showing an elevated proliferation index, increased clonogenic potential *in vitro* and enhanced
324 vascularity. In concordance with our preclinical data, research in mouse models of other human
325 cancers, in which the activation of the SHH pathway is also ligand dependent, has revealed that the
326 inhibition of this pathway (e.g. using vismodegib) is protumourigenic. For instance, the inhibition of
327 the SHH pathway in pancreatic ductal adenocarcinoma (PDAC) murine models either chemically or
328 genetically promotes tumour cell proliferation, undifferentiated phenotypes as well as increased
329 vascularity, resulting in greater tumour burden and shorter survival (Lee et al., 2014, Rhim et al.,
330 2014). Similarly, SHH pathway inhibition in colorectal cancer (CRC) murine models leads to higher
331 numbers of cells with tumour-initiating potential and accelerated tumour formation (Gerling et al.,

2016, Madison et al., 2005). Not unexpectedly, the inhibition of the hedgehog pathway in human PDAC and CRC was shown to yield rather disappointed results and patients either did not respond or, even worse, showed signs of faster cancer progression (Ko et al., 2016, Berlin et al., 2013, Catenacci et al., 2015). Moreover, a clinical trial using saridegib (an SMO inhibitor also known as IPI-926) in patients with PDAC was stopped due to increased tumourigenesis in the drug-treated group relative to the controls (Rimkus et al., 2016, Madden, 2012) (http://investors.infi.com/static-files/a2cbb418-8048-4f1f-94cc-dbbff91245be).

A limitation of the research presented here is the absence of corroborating genetic data to further elucidate the possible mechanisms by which SHH pathway inhibition leads to increased tumourigenesis in ACP. Unfortunately, *Hesx1*$^{Cre/+}$;*Shh*$^{flox/-}$ mice die at birth, which prevents such genetic study (i.e. the *Hesx1*$^{Cre/+}$;*Ctnnb1*$^{loxex3/+}$;*Shh*$^{flox/-}$ mice cannot be generated) (Carreno et al., 2017). Although ACP cellular models have been used, these have not been molecularly characterised and in our hands, the *CTNNB1* mutations that characterise the ACP tumours are lost in the culture cells. Nonetheless, our cellular and molecular characterisation suggest that common mechanisms underlie the protumourigenic effects of SHH pathway inhibition in ACP, PDAC and CRC. We propose that in addition to the angiogenic effects, such inhibition prevents exit of the cell cycle, resulting in higher numbers of proliferative tumour cells and accelerated tumourigenesis (Fig. 3G). In summary, using a clinically approved and widely employed SMO inhibitor in both the *Hesx1*$^{Cre/+}$;*Ctnnb1*$^{loxex3/+}$ mice and a human xenograft model, our research demonstrates that the inhibition of the SHH pathway has a tumour-promoting effect. We conclude that the use of vismodegib, and potentially other SMO inhibitors may be contraindicated in ACP patients.

ACKNOWLEDGEMENTS

We are grateful to Dr Dale Moulding for invaluable help in microscopy. We would like to thank the patients, their families and clinicians who have donated tissues to research. Funding for this research was provided by Cancer Research UK, Children's Cancer and Leukaemia Group, Children with Cancer UK (15/190), MRC (MR/M125/1), Brain Tumour Charity (SIGNAL and EVEREST), Great Ormond Street Hospital Children's Charity, Morgan Adams Foundation and National Institute of

 Accepted Manuscript published as ERC-18-0538.R1. Accepted for publication: 15-Jan-2019

Health Research Biomedical Research Centre at Great Ormond Street Hospital for Children NHS Foundation Trust and University College London. We also thank CR-UK support to the Cancer Imaging Centre at The Institute of Cancer Research and The Royal Marsden Hospital in association with the MRC and Department of Health (England) (C1060/A16464). S.H. is supported by a Wellcome Trust PhD Fellowship. J.R.A. is supported by a Cancer Research UK Clinical Research Training Fellowship. J.P.M.-B. is a Great Ormond Street Hospital for Children's Charity Principal Investigator.

COMPETING INTERESTS

The authors declare that they have no conflict of interest.

REFERENCES

ANDONIADOU, C. L., GASTON-MASSUET, C., REDDY, R., SCHNEIDER, R. P., BLASCO, M. A., LE TISSIER, P., JACQUES, T. S., PEVNY, L. H., DATTANI, M. T. & MARTINEZ-BARBERA, J. P. 2012. Identification of novel pathways involved in the pathogenesis of human adamantinomatous craniopharyngioma. *Acta Neuropathol,* 124**,** 259-71.

ANDONIADOU, C. L., MATSUSHIMA, D., MOUSAVY GHARAVY, S. N., SIGNORE, M., MACKINTOSH, A. I., SCHAEFFER, M., GASTON-MASSUET, C., MOLLARD, P., JACQUES, T. S., LE TISSIER, P., *et al.* 2013. Sox2(+) stem/progenitor cells in the adult mouse pituitary support organ homeostasis and have tumor-inducing potential. *Cell Stem Cell,* 13**,** 433-45.

ANDONIADOU, C. L., SIGNORE, M., SAJEDI, E., GASTON-MASSUET, C., KELBERMAN, D., BURNS, A. J., ITASAKI, N., DATTANI, M. & MARTINEZ-BARBERA, J. P. 2007. Lack of the murine homeobox gene Hesx1 leads to a posterior transformation of the anterior forebrain. *Development,* 134**,** 1499-508.

APPS, J. R., CARRENO, G., GONZALEZ-MELJEM, J. M., HASTON, S., JANI, N., HOLSKEN, A., PETTORINI, B., BEYNON, J. R., SUIMPSON, D. M., FRASER, H. C., *et al.* 2018. Tumour compartment transcriptomics demonstrate the activation of inflammatory and odontogenic programmes

in human adamantinomatous craniopharyngioma and identify novel therapeutic targets. *Acta Neuropathologica,* 135**,** 755-777.

BERLIN, J., BENDELL, J. C., HART, L. L., FIRDAUS, I., GORE, I., HERMANN, R. C., MULCAHY, M. F., ZALUPSKI, M. M., MACKEY, H. M., YAUCH, R. L., *et al.* 2013. A randomized phase II trial of vismodegib versus placebo with FOLFOX or FOLFIRI and bevacizumab in patients with previously untreated metastatic colorectal cancer. *Clin Cancer Res,* 19**,** 258-67.

BOULT, J. K. R., APPS, J. R., HOLSKEN, A., HUTCHINSON, J. C., CARRENO, G., D'ANIELSON, L. S., SMITH, L. M., BAUERTE, T., BUSLEI, R., BUCHFELDER, M., *et al.* 2017. Preclinical transgenic and patient-derived xenograft models recapitulate the radiological features of human adamantinomatous craniopharyngioma. *Brain Pathology 2017 doi: 10.1111/bpa.12525. [Epub ahead of print]*.

BRASTIANOS, P. K., TAYLOR-WEINER, A., MANLEY, P. E., JONES, R. T., DIAS-SANTAGATA, D., THORNER, A. R., LAWRENCE, M. S., RODRIGUEZ, F. J., BERNARDO, L. A., SCHUBERT, L., *et al.* 2014. Exome sequencing identifies BRAF mutations in papillary craniopharyngiomas. *Nature Genetics,* 46**,** 161-5.

BUSLEI, R., NOLDE, M., HOFMANN, B., MEISSNER, S., EYUPOGLU, I. Y., SIEBZEHNRUBL, F., HAHNEN, E., KREUTZER, J. & FAHLBUSCH, R. 2005. Common mutations of beta-catenin in adamantinomatous craniopharyngiomas but not in other tumours originating from the sellar region. *Acta Neuropathol,* 109**,** 589-97.

CARRENO, G., APPS, J., LODGE, E. J., PANOUSOPOULOS, L., HASTON, S., GONZALEZ-MELJEM, J. M., HAHN, H., ANDONIADOU, C. L. & MARTINEZ-BARBERA, J. P. 2017. Hypothalamic sonic hedgehog is required for cell specification and proliferation of LHX3/LHX4 pituitary embryonic precursors. *Development*.

CATENACCI, D. V., JUNTTILA, M. R., KARRISON, T., BAHARY, N., HORIBA, M. N., NATTAM, S. R., MARSH, R., WALLACE, J., KOZLOFF, M., RAJDEV, L., *et al.* 2015. Randomized Phase Ib/II Study

 Accepted Manuscript published as ERC-18-0538.R1. Accepted for publication: 15-Jan-2019

of Gemcitabine Plus Placebo or Vismodegib, a Hedgehog Pathway Inhibitor, in Patients With Metastatic Pancreatic Cancer. *J Clin Oncol,* 33**,** 4284-92.

DE SMAELE, E., FERRETTI, E. & GULINO, A. 2010. Vismodegib, a small-molecule inhibitor of the hedgehog pathway for the treatment of advanced cancers. *Curr Opin Investig Drugs,* 11**,** 707-18.

DONSON, A., APPS, J. R., GREISINGER, A. M., AMANI, V., WITT, D. A., ANDERSON, R. C., NIAZI, T. N., GRANT, G., SOUWEIDANE, M., JOHNSON, J. M., *et al.* 2017. Molecular Analyses Reveal Inflammatory Mediators in the Solid Component and Cyst Fluid of Human Adamantinomatous Craniopharyngioma. *Journal of Neuropathology and Experimental Neurology*.

GASTON-MASSUET, C., ANDONIADOU, C. L., SIGNORE, M., JAYAKODY, S. A., CHAROLIDI, N., KYEYUNE, R., VERNAY, B., JACQUES, T. S., TAKETO, M. M., LE TISSIER., *et al.* 2011. Increased Wingless (Wnt) signaling in pituitary progenitor/stem cells gives rise to pituitary tumors in mice and humans. *Proceedings of the National Academy of Sciences of the United States of America,* 108**,** 11482-7.

GERLING, M., BULLER, N. V., KIRN, L. M., JOOST, S., FRINGS, O., ENGLERT, B., BERGSTROM, A., KUIPER, R. V., BLAAS, L., WIELENGA, M. C., *et al.* 2016. Stromal Hedgehog signalling is downregulated in colon cancer and its restoration restrains tumour growth. *Nat Commun,* 7**,** 12321.

GOMES, D. C., JAMRA, S. A., LEAL, L. F., COLLI, L. M., CAMPANINI, M. L., OLIVEIRA, R. S., MARTINELLI, C. E., JR., ELIAS, P. C., MOREIRA, A. C., MACHADO., *et al.* 2015. Sonic Hedgehog pathway is upregulated in adamantinomatous craniopharyngiomas. *European Journal of Endocrinology / European Federation of Endocrine Societies,* 172**,** 603-8.

GONZALEZ-MELJEM, J. M., HASTON, S., CARRENO, G., APPS, J. R., POZZI, S., STACHE, C., KAUSHAL, G., VIRASAMI, A., PANOUSOPOULOS, L., MOUSAVY-GHARAVY, N. S., *et al.* 2017. Stem cell

437 senescence drives age-attenuated induction of pituitary tumours in mouse models of
438 paediatric craniopharyngioma. *Nat Commun,* 8**,** 1819.
439 GUMP, J. M., DONSON, A. M., BIRKS, D. K., AMANI, V. M., RAO, K. K., GRIESINGER, A. M.,
440 KLEINSCHMIDT-DEMASTERS, B. K., JOHNSTON, J. M., ANDERSON, R. C., ROSENFELD, *et al.*
441 2015. Identification of targets for rational pharmacological therapy in childhood
442 craniopharyngioma. *Acta Neuropathol Commun,* 3**,** 30.
443 HARADA, N., TAMAI, Y., ISHIKAWA, T., SAUER, B., TAKAKU, K., OSHIMA, M., TAKETO, M. M.,
444 MIYOSHI, H., MURAI, N. & OSHIMA, H. 1999. Intestinal polyposis in mice with a dominant
445 stable mutation of the beta-catenin gene. *EMBO Journal,* 18**,** 5931-42.
446 HASTON, S., POZZI, S., CARRENO, G., MANSHAEI, S., PANOUSOPOULOS, L., GONZALEZ-MELJEM, J. M.,
447 APPS, J. R., VIRASAMI, A., THAVARAJ, S., GUTTERIDGE, A., *et al.* 2017. MAPK pathway control
448 of stem cell proliferation and differentiation in the embryonic pituitary provides insights into
449 the pathogenesis of papillary craniopharyngioma. *Development,* 144**,** 2141-2152.
450 HOLSKEN, A., SILL, M., MERKLE, J., SCHWEIZER, L., BUCHFELDER, M., FLITSCH, J., FAHLBUSCH, R.,
451 METZLER, M., KOOL, M., PFISTER, S. M., VON DEIMLING, A., *et al.* 2016. Adamantinomatous
452 and papillary craniopharyngiomas are characterized by distinct epigenomic as well as
453 mutational and transcriptomic profiles. *Acta Neuropathol Commun,* 4**,** 20.
454 KARAVITAKI, N. & WASS, J. A. 2008. Craniopharyngiomas. *Endocrinol Metab Clin North Am,* 37**,** 173-
455 93, ix-x.
456 KARP, N. A., MEEHAN, T. F., MORGAN, H., MASON, J. C., BLAKE, A., KURBATOVA, N., SMEDLEY, D.,
457 JACOBSEN, J., MOTT, R. F., IYER, V., *et al.* 2015. Applying the ARRIVE Guidelines to an In Vivo
458 Database. *PLoS Biol,* 13**,** e1002151.
459 KATO, K., NAKATANI, Y., KANNO, H., INAYAMA, Y., IJIRI, R., NAGAHARA, N., MIYAKE, T., TANAKA, M.,
460 ITO, Y., AIDA, N., *et al.* 2004. Possible linkage between specific histological structures and
461 aberrant reactivation of the Wnt pathway in adamantinomatous craniopharyngioma. *J*
462 *Pathol,* 203**,** 814-21.

 Accepted Manuscript published as ERC-18-0538.R1. Accepted for publication: 15-Jan-2019

463 KO, A. H., LOCONTE, N., TEMPERO, M. A., WALKER, E. J., KATE KELLEY, R., LEWIS, S., CHANG, W. C.,
464 KANTOFF, E., VANNIER, M. W., CATENACCI, D. V., *et al.* 2016. A Phase I Study of FOLFIRINOX
465 Plus IPI-926, a Hedgehog Pathway Inhibitor, for Advanced Pancreatic Adenocarcinoma.
466 *Pancreas,* 45**,** 370-5.
467 LEE, J. J., PERERA, R. M., WANG, H., WU, D. C., LIU, X. S., HAN, S., FITAMANT, J., JONES, P. D.,
468 GHANTA, K. S., KAWANO, *et al.* 2014. Stromal response to Hedgehog signaling restrains
469 pancreatic cancer progression. *Proc Natl Acad Sci U S A,* 111**,** E3091-100.
470 MADDEN, J. I. 2012. Infinity Reports Update from Phase 2 Study of Saridegib Plus Gemcitabine in
471 Patients with Metastatic Pancreatic Cancer. *Business Wire*.
472 MADISON, B. B., BRAUNSTEIN, K., KUIZON, E., PORTMAN, K., QIAO, X. T. & GUMUCIO, D. L. 2005.
473 Epithelial hedgehog signals pattern the intestinal crypt-villus axis. *Development,* 132**,** 279-89.
474 MULLER, H. L., MERCHANT, T. E., PUGET, S. & MARTINEZ-BARBERA, J. P. 2017. New outlook on the
475 diagnosis, treatment and follow-up of childhood-onset craniopharyngioma. *Nat Rev*
476 *Endocrinol,* 13**,** 299-312.
477 RHIM, A. D., OBERSTEIN, P. E., THOMAS, D. H., MIREK, E. T., PALERMO, C. F., SASTRA, S. A., DEKLEVA,
478 E. N., SAUNDERS, T., BECERRA, C. P., TATTERSALL *et al.* 2014. Stromal elements act to
479 restrain, rather than support, pancreatic ductal adenocarcinoma. *Cancer Cell,* 25**,** 735-47.
480 RIMKUS, T. K., CARPENTER, R. L., QASEM, S., CHAN, M. & LO, H. W. 2016. Targeting the Sonic
481 Hedgehog Signaling Pathway: Review of Smoothened and GLI Inhibitors. *Cancers (Basel),* 8.
482 SEKINE, S., SHIBATA, T., KOKUBU, A., MORISHITA, Y., NOGUCHI, M., NAKANISHI, Y., SAKAMOTO, M.
483 & HIROHASHI, S. 2002. Craniopharyngiomas of adamantinomatous type harbor beta-catenin
484 gene mutations. *Am J Pathol,* 161**,** 1997-2001.
485 SEKULIC, A., MIGDEN, M. R., BASSET-SEGUIN, N., GARBE, C., GESIERICH, A., LAO, C. D., MILLER, C.,
486 MORTIER, L., MURRELL, D. F., HAMID, O., *et al.* 2017. Long-term safety and efficacy of
487 vismodegib in patients with advanced basal cell carcinoma: final update of the pivotal
488 ERIVANCE BCC study. *BMC Cancer,* 17**,** 332.

SEKULIC, A., MIGDEN, M. R., ORO, A. E., DIRIX, L., LEWIS, K. D., HAINSWORTH, J. D., SOLOMON, J. A., YOO, S., ARRON, S. T., FRIEDLANDER, *et al.* 2012. Efficacy and safety of vismodegib in advanced basal-cell carcinoma. *N Engl J Med,* 366**,** 2171-9.

STACHE, C., HOLSKEN, A., SCHLAFFER, S. M., HESS, A., METZLER, M., FREY, B., FAHLBUSCH, R., FLITSCH, J., BUCHFELDER, M. & BUSLEI, R. 2015. Insights into the infiltrative behavior of adamantinomatous craniopharyngioma in a new xenotransplant mouse model. *Brain Pathol,* 25**,** 1-10.

THEUNISSEN, J. W. & DE SAUVAGE, F. J. 2009. Paracrine Hedgehog signaling in cancer. *Cancer Research,* 69**,** 6007-10.

WONG, H., ALICKE, B., WEST, K. A., PACHECO, P., LA, H., JANUARIO, T., YAUCH, R. L., DE SAUVAGE, F. J. & GOULD, S. E. 2011. Pharmacokinetic-pharmacodynamic analysis of vismodegib in preclinical models of mutational and ligand-dependent Hedgehog pathway activation. *Clinical Cancer Research,* 17**,** 4682-92.

WORKMAN, P., ABOAGYE, E. O., BALKWILL, F., BALMAIN, A., BRUDER, G., CHAPLIN, D. J., DOUBLE, J. A., EVERITT, J., FARNINGHAM, D. A., GLENNIE, M. J., *et al.* 2010. Guidelines for the welfare and use of animals in cancer research. *British Journal of Cancer,* 102**,** 1555-77.

 Accepted Manuscript published as ERC-18-0538.R1. Accepted for publication: 15-Jan-2019

Figure legends

Figure 1.

Inhibition of the SHH pathway in *Hesx1$^{Cre/+}$;Ctnnb1$^{lox(ex3)/+}$* mice, a murine model of human adamantinomatous craniopharyngioma (ACP), results in reduced median survival.

(A) Double immunofluorescence on formalin-fixed paraffin-embedded (FFPE) histological sections of human ACP showing the expression of SHH in the β-catenin-accumulating cell clusters. Scale bar: 25 μm. **(B)** Double immunofluorescence on FFPE histological sections of *Hesx1$^{Cre/+}$;Ctnnb1$^{lox(ex3)/+}$* tumoural pituitaries revealing the expression of SHH in the β-catenin-accumulating cell clusters at specific time points of postnatal life. Note the overall reduction in SHH staining from one to 8 weeks of age. Scale bar: 50 μm **(C)** qRT-PCR analysis showing the up-regulation of *Shh* and the target pathway gene *Gli1* in the tumoural pituitaries of the *Hesx1$^{Cre/+}$;Ctnnb1$^{lox(ex3)/+}$* ACP mouse model compared with *Ctnnb1$^{lox(ex3)/+}$* controls at specific ages (*Shh*: one week, 134-fold; four weeks, 125-fold; 8 weeks, 68-fold; *Gli1*: one week, 15.3-fold, p=0.018; four weeks, 8.7-fold, p<0.0001; eight weeks, 4.9-fold, p<0.0001; (n=3-5 tumoural pituitaries per time point, Student's t-test). **(D)** qRT-PCR analysis of *Gli1* expression levels in *Hesx1$^{Cre/+}$;Ctnnb1$^{loxex3/+}$* tumoural and *Ctnnb1$^{lox(ex3)/+}$* control pituitaries treated twice daily with vismodegib (100 mg/kg) for one week in comparison with vehicle-treated and untreated mice. There is an overall reduction in *Gli1* expression levels upon vismodegib treatment, which does not reach significance possibly due to the marked variability in *Gli1* expression levels in the untreated and vehicle treated controls (untreated: 2.1-fold, n=7 mice; vehicle: 2.5-fold, n=8 mice; vismodegib: 1.5-fold, n=8 mice; p=0.35, One-way ANOVA). **(E)** Schematic diagram of the preclinical trial. Age-matched *Hesx1$^{Cre/+}$;Ctnnb1$^{loxex3/+}$* male mice are dosed twice daily with 100 mg/kg vismodegib (11 mice) or vehicle (12 mice) for 28 days starting around 4-5 weeks of age (56 doses). At the end of treatment, mice are left untreated and monitored by MRI every two weeks and at the humane end point. **(F)** Kaplan-Meier analysis showing a reduction in median survival in the vismodegib-treated (11.9 weeks, n=11, red line) relative to the vehicle-treated mice (33.3 weeks, n=12, blue line; p=0.049, Mantel-Cox (log-rank) test). Data represent the mean ± SD.

Figure 2.

Highly proliferative and vascularised tumours are formed upon treatment with vismodegib in the *Hesx1$^{Cre/+}$;Ctnnb1$^{lox(ex3)/+}$* ACP mouse model.

(A) Axial T2-weighted MRI scans of vismodegib and vehicle -treated *Hesx1$^{Cre/+}$;Ctnnb1$^{lox(ex3)/+}$* mice at the level of the brain (two examples of each are shown, labels indicate days after the end of treatment). Note the expansion of the pituitary to form a solid tumour component (arrows) and the development of hyperintense cysts and hypointense haemorrhagic regions in both vehicle and vismodegib -treated groups. **(B)** Hematoxylin-eosin (H&E) staining of FFPE histological sections of *Hesx1$^{Cre/+}$;Ctnnb1$^{loxex3/+}$* tumours showing similar histology between experimental groups. Immunofluorescence revealing the increased expression of Ki67 (proliferative marker), pHH3 (mitotic marker) and Endomucin (endothelial marker) in vismodegib-treated tumours compared with the vehicle-treated controls. Scale bar: 50 μm. **(C)** The Ki67 proliferation index (fraction of Ki67+ve cells out of total DAPI+ve cells) is increased in the vismodegib-treated group (vehicle: 27.4±5.5%, n=9 tumours; vismodegib: 41.3±7.%, n=10 tumours; p=0.0002, Student's t-test). **(D)** The mitotic index (fraction of pHH3+ve cells out of total DAPI+ve cells) is elevated upon vismodegib treatment (vehicle: 3.6±0.8%, n=9 tumours; vismodegib: 6.5±3%; n=10 tumours; p=0.016, Student's t-test). **(E)** Vasculature is increased in the vismodegib-treated group as assessed by immunofluorescence against Endomucin (total fluorescent area: vehicle: 5.4±1.4%; vismodegib: 7.8±2%; n=6 tumours per group; p=0.0319, Student's t-test). **(F)** Doubling time of the solid component of the tumours, as calculated from contiguous MRI scans, is reduced by 47% upon vismodegib treatment (vehicle: 15.3±3 days, n=7 tumours; vismodegib: 8.1±1 days, n=6 tumours; p=0.044, Student's t-test). Data represent mean ± SD.

Figure 3.

Vismodegib treatment results in higher numbers of clonogenic cells and premature formation of tumours.

 Accepted Manuscript published as ERC-18-0538.R1. Accepted for publication: 15-Jan-2019

(A) Diagram of the experimental approach. Four-week old *Hesx1*$^{Cre/+}$;*Ctnnb1*$^{loxex3/+}$ male mice are dose twice daily with either vismodegib (100mg/kg) or vehicle for one week, after which pituitaries are dissected and analysed both histologically and in a clonogenic assay. **(B)** H&E staining on FFPE histological sections of vehicle and vismodegib -treated mice showing the presence of large tumoural lesions (arrows) and cysts (arrowheads) in vismodegib-treated animals. The control pituitaries show smaller cysts (arrowheads) and no tumour lesions are detectable (n=3 pituitaries per group). This is in agreement with our previous observations of a latency period of around 17 weeks for tumour formation (Boult et al., 2017)(Boult et al. 2017). Scale bar: 100 μm. **(C)** The premature tumour lesions are Synaptophysin-ve (black arrow) by immunohistochemistry, and highly proliferative, as assessed by immnufluorescence against Ki67 (white arrow). **(D)** Quantitative analysis demonstrates the higher Ki67 proliferative index upon vismodegib treatment **(**vehicle: 3.2±1.2%; vismodegib: 8.8±1.0%, n=3 pituitaries per group; p=0.0029, Student's t-test). Scale bar: 200 μm. **(E)** Quantification of the clonogenic potential of pituitaries from mice treated with either vehicle or vismodegib (n=3 pituitaries per group). Note that vismodegib treatment results in drastic increase in clonogenic potential of nearly 90% relative to the vehicle controls (vehicle: 2597±98 colonies; vismodegib: 4924±167 colonies, n=3 pituitaries per group; p=0.0003, Student's t-test). **(F)** Representative examples of plates seeded with 2000, 4000 and 8000 pituitary cells from vehicle and vismodegib -treated *Hesx1*$^{Cre/+}$;*Ctnnb1*$^{loxex3/+}$ mice. Plates are stained with haematoxylin. **(G)** Schematic summary of main findings. The expression of oncogenic β-catenin in *Hesx1*$^{Cre/+}$;*Ctnnb1*$^{loxex3/+}$ mice results in formation of β-catenin-accumulating cell clusters, which secrete SHH and activate the pathway in surrounding tumour cells inducing a more quiescent phenotype characterised by exit of a proliferative, Ki67+ve state. vismodegib-mediated inhibition of the SHH pathway leads to more proliferative and aggressive tumours. All graph bars represent mean ± SD.

Figure 4.

Inhibition of the SHH pathway leads to increased tumour cell proliferation in both explant cultures and xenograft models of human ACP.

(A) Schematic diagram of the explant culture experiments. Three ACP tumour samples were cut into 1-2 mm^3 cubes and cultured in the presence of vismodegib (100 μM) or vehicle (DMSO). Four biological replicates were performed for each analysis (i.e. four pieces of tumours per treatment). **(B)** qRT-PCR analysis showing the overall inhibition of the SHH pathway as assessed by a variable reduction in *GLI1*, *PTCH1* and *SHH* expression upon vismodegib treatment in three human ACP tumours. One sample did not show reduction of *GLI1*, but both PTCH1 and SHH expression were reduced. **(C)** Double immunofluorescence on FFPE histological sections showing increased expression of Ki67+ve in the human ACP explants cultured in the presence of vismodegib relative to the DMSO-treated controls. Scale bar: 25 μm. **(D)** Quantitative analysis revealing a higher Ki67+ve proliferative index in vismodegib compared with vehicle -treated explants (vehicle: 5.1±3%; vismodegib: 38.7±12%; n=3 tumours per group; p=0.0085, Student's t-test). **(E)** Schematic diagram of the human ACP xenograft experiments. Two human ACP tumours were cut into 1-2mm^3 and implanted into the cortex of 20 immunosuppressed mice (11 animals with Tumour 1 and 9 with Tumour 2). Three months later, mice were randomised into two groups of 10 mice each and dosed twice daily with 100 mg/kg vismodegib or vehicle for 21 days, after which brains were dissected and analysed histologically. **(F)** Double immunofluorescent staining revealing the presence of Ki67+ve cells (arrows) in the proximity of β-catenin-accumulating cell clusters (asterisks) in both vismodegib and vehicle -treated xenografted human ACP tumours. Scale bar: 25 μm. **(G)** Quantitative analysis showing an elevation of the Ki67 proliferative index in the xenografted tumours upon treatment with vismodegib (vehicle: 1.8±0.5%, n=3 tumour-bearing mice; vismodegib: 12.7±2%, n=4 tumour-bearing mice; $p<0.0001$, Student's t-test). All graph bars represent mean ± SD.

 Accepted Manuscript published as ERC-18-0538.R1. Accepted for publication: 15-Jan-2019

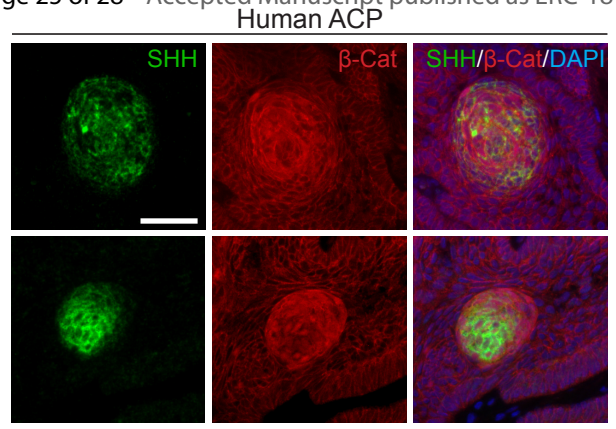

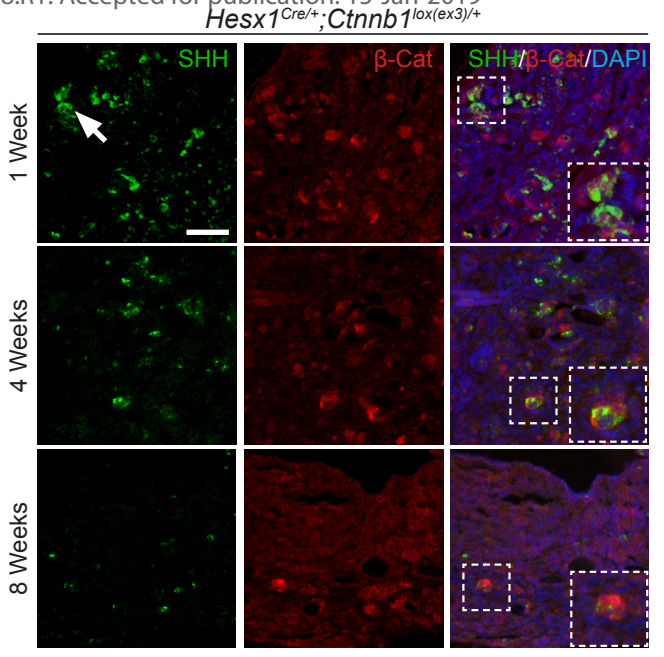

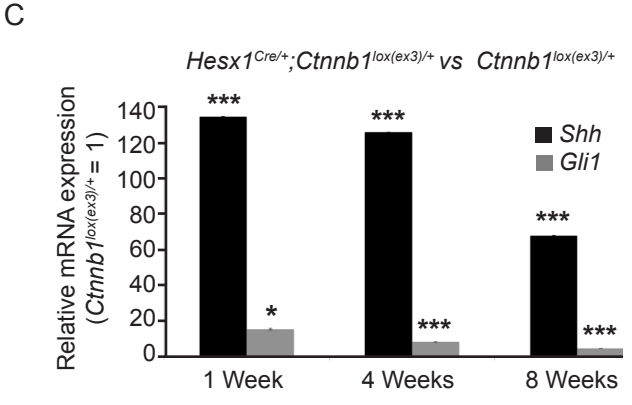

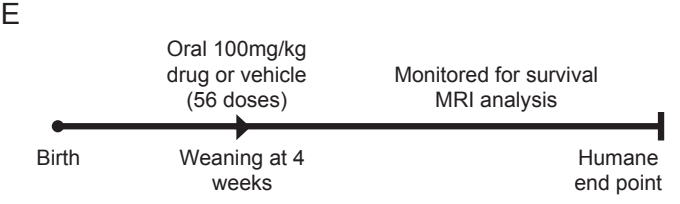

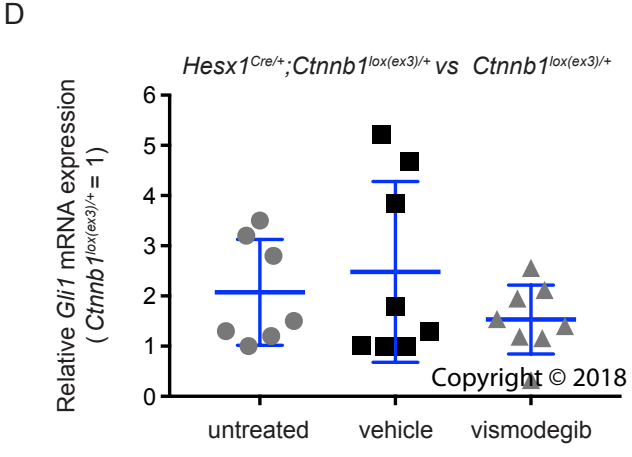

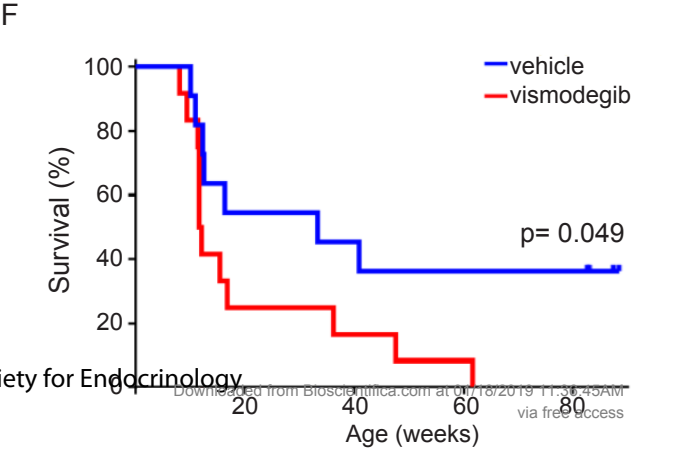

A

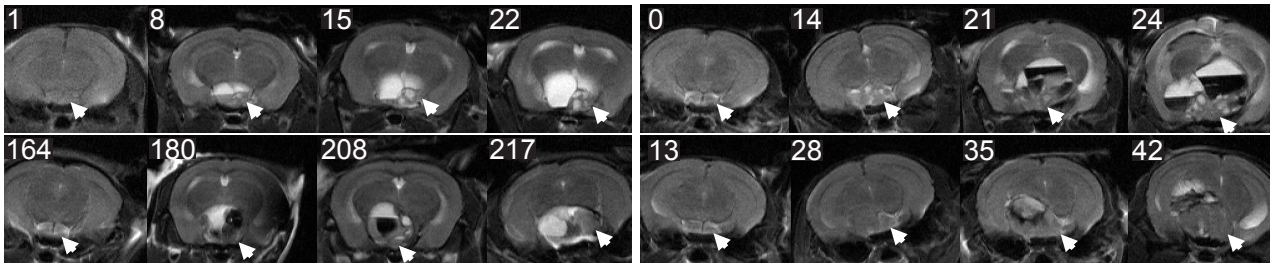

B

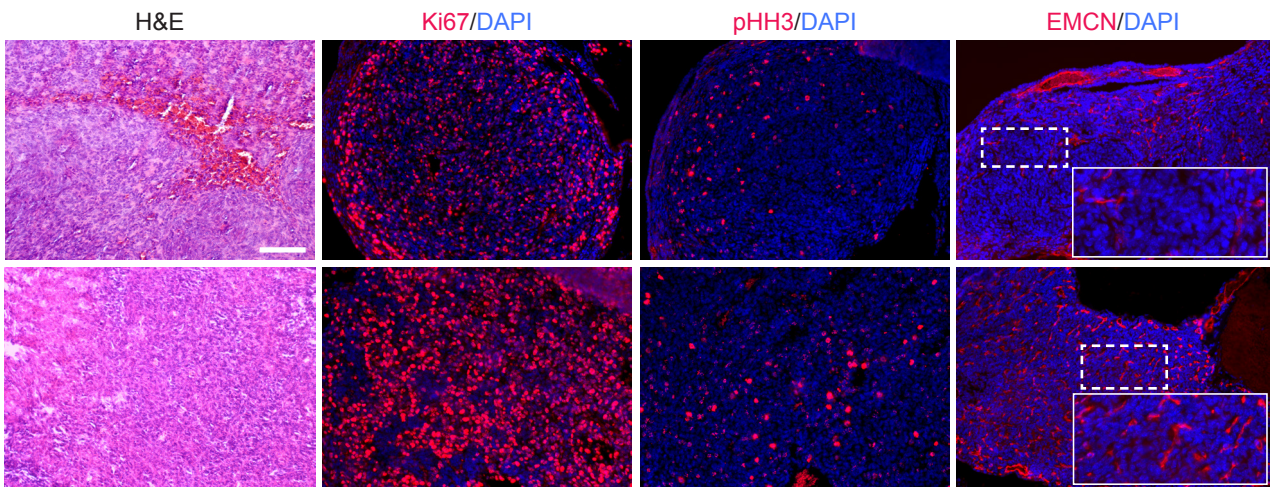

C

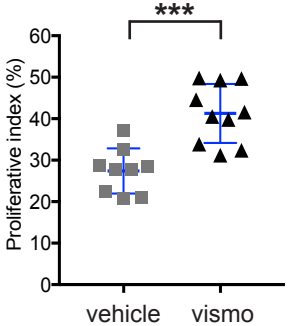

D

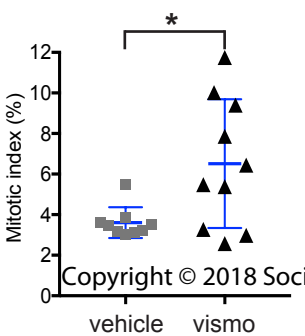

E

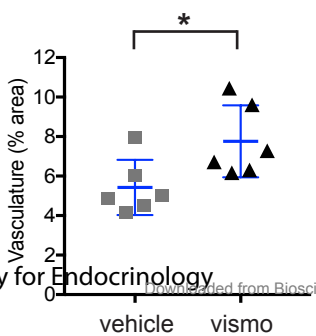

F

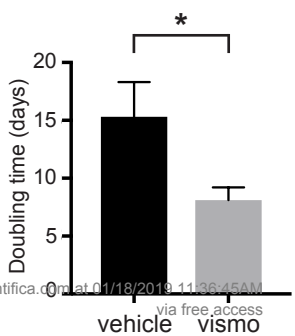

Accepted Manuscript published as ERC-18-0538.R1. Accepted for publication: 15-Jan-2019

A

Twice daily oral treatment
(vismodegib or vehicle)

Hesx1$^{Cre/+}$;*Ctnnb1*$^{lox(ex3)/+}$
(4 wk-old males)

7 days

Histological and clonogenic-potential analyses

B

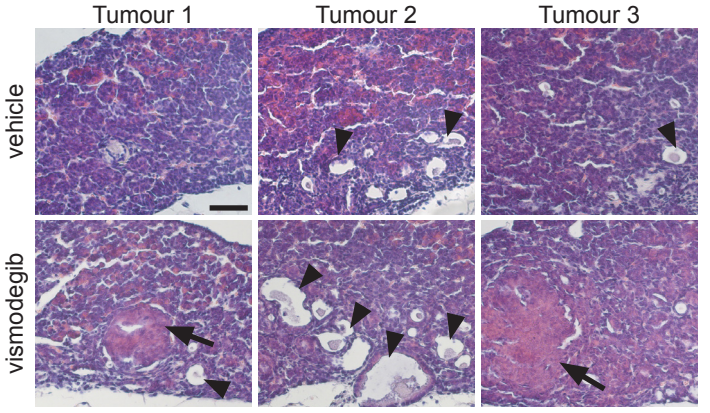

C

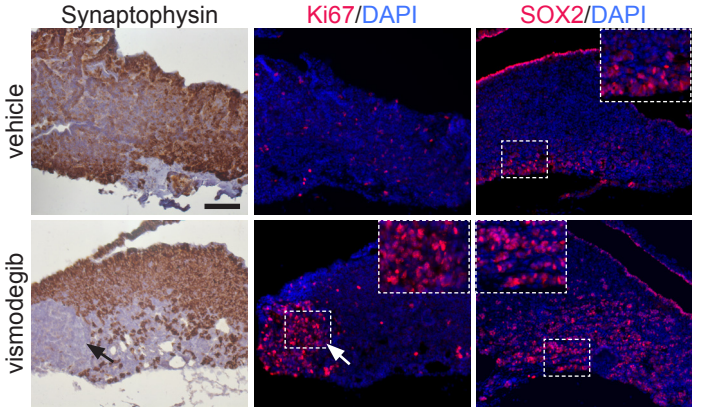

D

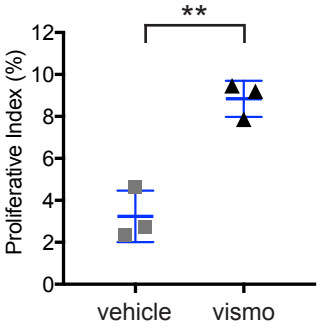

E

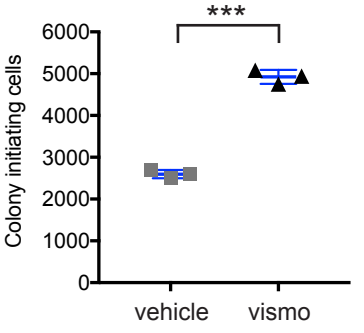

F

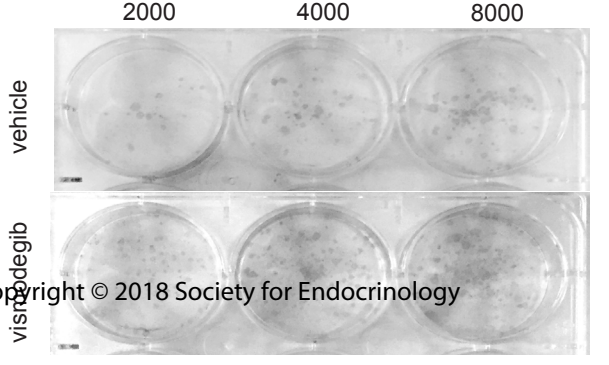

G

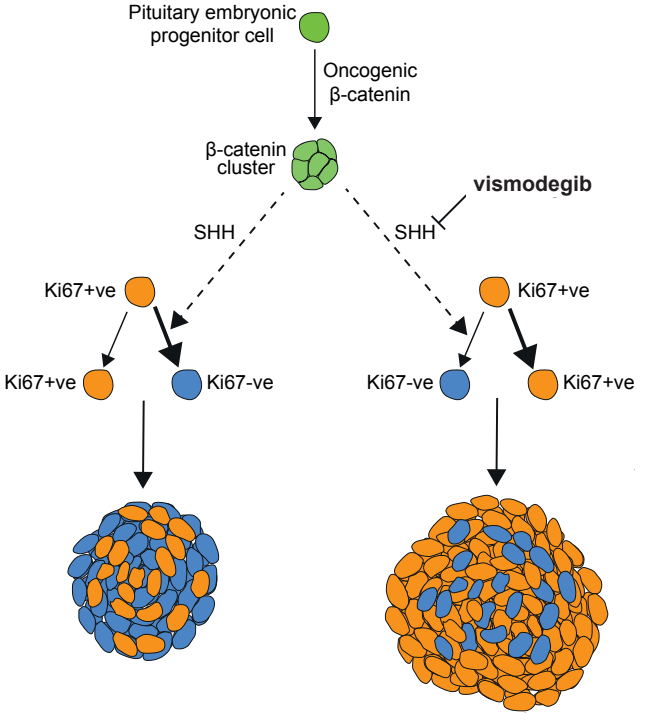

A

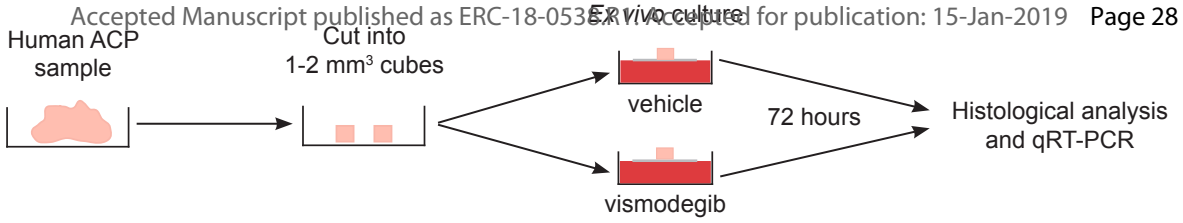

B

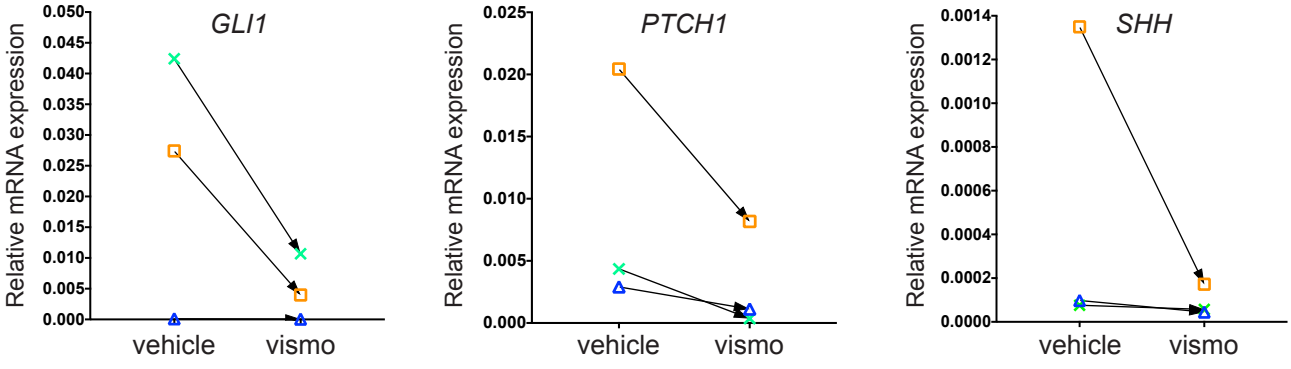

C

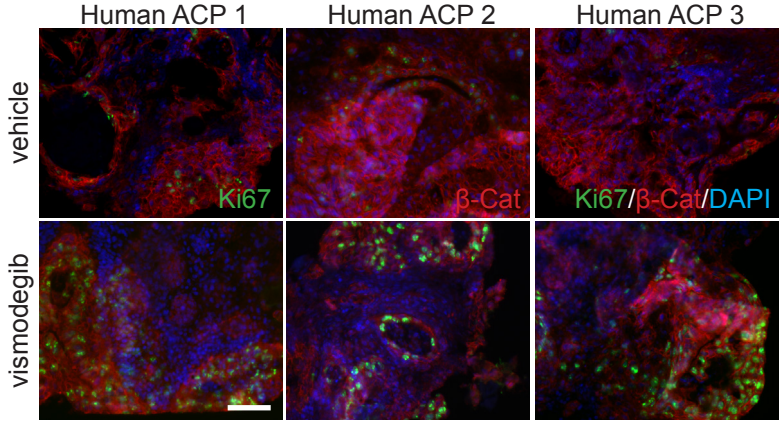

D

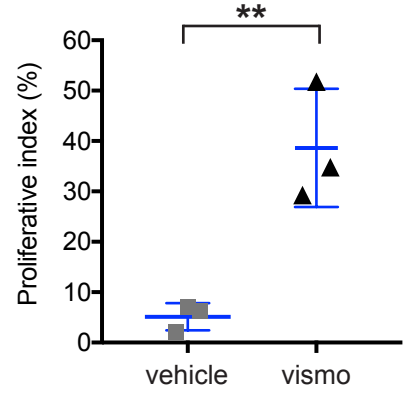

E

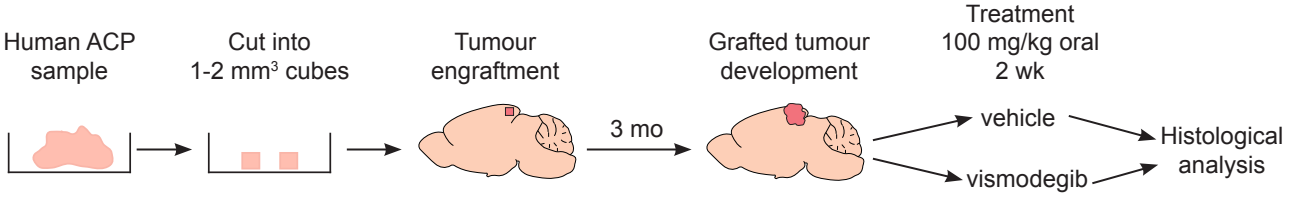

F

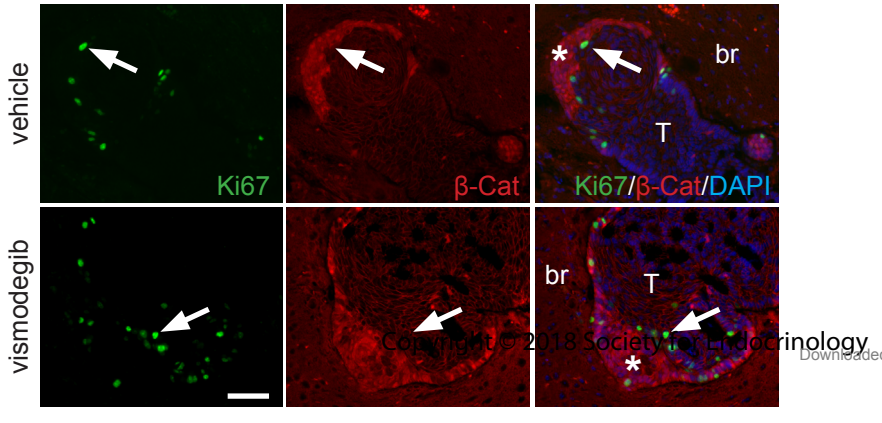

G